







Large variation in superconducting transition temperature in the $\text{Nb}_x\text{Bi}_{2-x}\text{Se}_3$ system

Simone M. Keyv ¹, Laura Wollesen ¹, Kirstine J. Dalgaard ¹, Yu-Te Hsu ²,
Steffen Wiedmann ² and Martin Bremholm ^{1,*}

¹*Department of Chemistry, Interdisciplinary Nanoscience Center (iNANO), Aarhus University, 8000 Aarhus C, Denmark*

²*High Field Magnet Laboratory and Institute for Molecules and Materials, Radboud University, 6525 ED Nijmegen, Netherlands*



(Received 25 August 2023; revised 2 March 2024; accepted 4 April 2024; published 2 May 2024)

Samples synthesized as Nb substituted onto Bi sites from the nominal composition of $\text{Nb}_x\text{Bi}_{2-x}\text{Se}_3$ resulted in superconducting critical temperatures (T_c 's) in transport measurements reaching 5.6 K and 5.4 K, for $x = 0.2$ and 0.25, respectively. All, significantly higher than reported in earlier studies of compositions aiming at Nb intercalation $\text{Nb}_x\text{Bi}_2\text{Se}_3$. Bulk susceptibility showed lower responses for powders with a large variety, including T_c 's ranging from 1.8 K to 4.5 K. Magnetotransport experiments were conducted with angular dependence at the High Field Magnet Laboratory (HFML). Clear Shubnikov–de Haas oscillations were observed in all substituted samples, and a thorough study of the angular dependence of the Shubnikov–de Haas frequencies is presented together with estimates of the Fermi energy (E_F). All samples contain the phases of Bi_2Se_3 and the misfit compound $(\text{BiSe})_{1.1}\text{NbSe}_2$. However, only some areas of the crystal boules contain the third phase of BiSe, and the calculated niobium contents from the nominal composition and the results from the phase analysis show large variations. The results obtained on these substituted samples are compared to the more studied Nb-doped Bi_2Se_3 stoichiometry, thereby giving further insight into this system currently under high interest.

DOI: [10.1103/PhysRevMaterials.8.054801](https://doi.org/10.1103/PhysRevMaterials.8.054801)

I. INTRODUCTION

Topological insulators and Dirac materials have been intensely studied since the first discovery not many decades ago [1–4], with Bi_2Se_3 showcasing remarkable electronic properties. Upon doping some of these topological insulators such as Bi_2Se_3 with Cu [5–8], Sr [9–11], or Nb [12–16], become superconducting. It is hypothesized that topological superconductivity might be realized in these systems [17,18]. These proposed topological superconductors are of considerable interest for hosting Majorana quasiparticles, which might be applicable in topological quantum computation [19]. Therefore, much effort is being put into investigating candidate materials for topological superconductivity [20].

Despite the growing interest in doped Bi_2Se_3 systems, a convincing mechanism behind the occurrence of superconductivity has yet to be reported. The first discovered Cu-doped system is widely believed to become superconducting upon intercalation of the Cu atoms into the layered structure of Bi_2Se_3 in the weakly bound van der Waals gap of the quintuple layers [6]. Results from electrochemically intercalating Cu into the host structure [21] further underline this hypothesis. Sr-doped Bi_2Se_3 has been suggested to become superconducting by similar effects [9], until it was proposed that Sr atoms are possibly doped at interstitial locations in the structure instead [22]. The interest peaked when the Nb-doped case was later reported to display even better superconducting abilities than the two previous systems [12]. Again, the intercalation model was suggested and widely appreciated as the

mechanism behind superconductivity [12,15]. However, there were some reports on the appearance of an “impurity phase” with low content, but it was not believed to have any influence on the superconductivity [23]. They observed that with smaller doping levels the impurity was present, and at higher doping levels (\geq wt.%), BiSe also appeared in large amounts together with a possible substitution of Bi with Nb rather than intercalation.

Later, we observed that the “impurity phase” was the misfit compound $(\text{BiSe})_{1.1}\text{NbSe}_2$, which appeared in every superconducting sample [14]. In 1989 this was first reported as BiNbSe_3 [24]. However, in 1992 it was recognized as the misfit layer compound, $(\text{BiSe})_{1.10}\text{NbSe}_2$ [25], consisting of alternating layers of cubic BiSe and NbSe_2 as Se-Nb-Se stacks. The misfit phase was then later discovered to be superconducting, with a T_c of 2.4 K [26]. Concurrently, it was rationalized that the origin behind superconductivity in the Nb-doped Bi_2Se_3 system is due to the presence of the misfit phase, both in our work [14] and by others [27]. Working further with these samples in our group then led to a study of the local structure of Nb-doped Bi_2Se_3 [28]. The local surrounding environment was investigated using the x-ray absorption fine structure (XAFS) technique. Here samples with nominal contents of $\text{Nb}_{0.25}\text{Bi}_2\text{Se}_3$ (Nb-doped) and $\text{Nb}_{0.25}\text{Bi}_{1.75}\text{Se}_3$ (Nb-substituted) were studied. The results showed that the local structure around Nb could all be assigned to NbSe_2 in $(\text{BiSe})_{1.1}\text{NbSe}_2$. The $\text{Nb}_{0.25}\text{Bi}_{1.75}\text{Se}_3$ showed a T_c at 1.8 K, which has not been reported elsewhere. Presently, insight into the formation of misfit during the synthesis was also published from our group, revealing how the misfit layer compound is unavoidable and unquestionably linked to the occurrence of superconductivity in the doped $\text{Nb}_x\text{Bi}_2\text{Se}_3$ samples [29].

*bremholm@chem.au.dk

TABLE I. Sample overview with the content of Nb(x) in the nominal composition of $\text{Nb}_x\text{Bi}_{2-x}\text{Se}_3$ or $\text{Nb}_x\text{Bi}_2\text{Se}_3$, together with synthesis conditions on the maximum treatment temperature and cooling rate. S1 is the sample that was first published by Dalgaard *et al.* [28] (referred to as S2 in that publication). S1 was synthesized before the others and did not have the two days prereaction as the rest did, which was later found to optimize melting.

Sample	Nb(x)	Treatment	Stoichiometric content
<i>Substituted samples</i>			
S1	0.25	900 °C, 6 °C/h	$\text{Nb}_{0.25}\text{Bi}_{1.75}\text{Se}_3$
S2	0.25	950 °C, 4 °C/h	$\text{Nb}_{0.25}\text{Bi}_{1.75}\text{Se}_3$
S3	0.20	950 °C, 4 °C/h	$\text{Nb}_{0.20}\text{Bi}_{1.80}\text{Se}_3$
S4	0.10	950 °C, 4 °C/h	$\text{Nb}_{0.10}\text{Bi}_{1.90}\text{Se}_3$
<i>Nb-doped Bi_2Se_3 samples</i>			
S5	0.25	950 °C, 4 °C/h	$\text{Nb}_{0.25}\text{Bi}_2\text{Se}_3$

This study revisits the previous suggestion of Nb being substituted into the Bi_2Se_3 structure on the Bi sites. The system is found to display inhomogeneities and was investigated with the determination of the susceptibility from magnetic measurements and phase contents from powder x-ray diffraction (PXRD). Furthermore, the atypical superconducting transition in the already investigated sample from Dalgaard *et al.* [28] was also discovered in new samples with an in-depth study of the magnetoresistance properties at higher magnetic fields (up to 30 T). Five samples are used for our investigations in this study, one being the same as in [28] (S1, note: in the reference this sample is S2). The four new samples have the stoichiometry of Nb substituting into the Bi sites ($\text{Nb}_x\text{Bi}_{2-x}\text{Se}_3$, called S2–S4) and one Nb-doped for comparison ($\text{Nb}_{0.25}\text{Bi}_2\text{Se}_3$, called S5). An overview of the samples is displayed in Table I. We will present the combined study with results from transport, magnetotransport, susceptibility, and phase analysis to gain new insights into the effect of the structural details behind the properties observed for the system.

II. EXPERIMENTAL METHODS

Bulk samples (around 3 g) with a nominal composition of $\text{Nb}_x\text{Bi}_{2-x}\text{Se}_3$ ($x = 0.10, 0.20, \text{ and } 0.25$) and $\text{Nb}_{0.25}\text{Bi}_2\text{Se}_3$ were synthesized through a melt growth method, as also described elsewhere [14]. Powders of Bi (99.999%), Se (99.999%), and Nb (99.99%) were mixed in a stoichiometric ratio, evacuated to 10^{-4} mbar, and sealed in a quartz ampoule. Prereaction was conducted at 900 °C–950 °C (50 °C/h) for 2 days (except for S1), 24 hours again at 900 °C–950 °C (50 °C/h), followed by slow cooling to 650 °C (4 °C–6 °C/h), before quenching in ice water. Details are displayed in Table I, and further information is given in the Supplemental Material (SM) [30].

Magnetotransport experiments were conducted at the High Field Magnet Laboratory (HFML), Nijmegen, on cleaved samples of typically 100–300 μm thickness, with a length and width < 3 mm. Wires were attached to the samples with conducting silver paste. Experiments were performed in a vacuum tube equipped with an inner vacuum chamber (IVC) down to

1.3 K and conducted at the resistive (Bitter) magnet up to 30 T using standard lock-in detection techniques with an excitation current of 1 mA. The magnetoresistance was measured in a magnetic field B_{\perp} perpendicular to the flat sample (parallel to the c axis of the Bi_2Se_3 structure) and B_{\parallel} parallel to the flat sample, perpendicular to the current path.

Powders were characterized by powder x-ray diffraction (PXRD) on a Rigaku SmartLab diffractometer with $\text{Cu K}\alpha 1$ ($\lambda = 1.5406$ Å) radiation. The potential Seebeck microprobe (PSM) was utilized to measure the spatially resolved Seebeck coefficient on the surface of a sample at room temperature. A heated tip induces a local temperature gradient on the sample as the temperature and potential difference are measured by two T-type thermocouples [31]. Magnetic susceptibility measurements were performed with a physical property measurement system (PPMS) with the vibrating sample magnetometer (VSM) option in the range from 1.75 to 10 K (zero-field cooled, ZFC). All $T_{c(\text{onset})}$ values for powders are determined by linearly extrapolating the upper and lower parts of the curve around the drop in susceptibility values and determining the intercept as the $T_{c(\text{onset})}$. For the resistivity measurements, $T_{c(\text{crystal})}$ is determined as the first change in the first derivative.

III. RESULTS

A. Single crystals

Single crystals in the substitution system with $\text{Nb}_x\text{Bi}_{2-x}\text{Se}_3$ were studied, as each crystal boule was divided into areas and named alphabetically. A complete overview of the crystal areas can be found in the Supplemental Material (SM) [30] in Table I, together with an illustration in Fig. S1. The areas were split in two; one was kept single crystalline for the transport measurements, and the rest was ground to a fine powder to ensure that the same areas could be investigated by several techniques.

Transport experiments revealed superconductivity in the newly made substituted samples (S2–S5), as displayed in Fig. 1. A large variety of the properties were compared to S1 [already published in [28], with a T_c of 1.8 K, as S2(2-B)]. The critical temperatures, ranging from 3.3 K up to 5.6 K, have, to our knowledge, never been reported for the system with a nominal composition of $\text{Nb}_x\text{Bi}_2\text{Se}_3$. The results from the S3-B single crystal are displayed in Fig. 1(a) in the inset from 300 to 4.2 K, showing metallic behavior above the superconducting transition. T_c is the onset of superconductivity, determined to be 5.6 K for S3-B. The residual resistance ratio (RRR) [32] underlines how the crystal quality of these samples closely resembles that of the undoped Bi_2Se_3 (see details in the SM [30]).

In Fig. 1(b), the sample S3-B exhibits the largest decrease in the resistivity signal upon entering the superconducting state. However, it does not reach zero at the lowest temperature of 1.7 K. For S2-C, the T_c is determined to be 5.4 K [see zoom-in of Fig. 1(c)], though it is a small change in the resistivity [compared to the others in Fig. 1(b)]. The S2 and S3 crystals are from samples made with 25% and 20% Nb substituted with Bi, respectively (see Table I). The sample S4-C, with a 10% Nb substitution [Fig. 1(b)], exhibits a

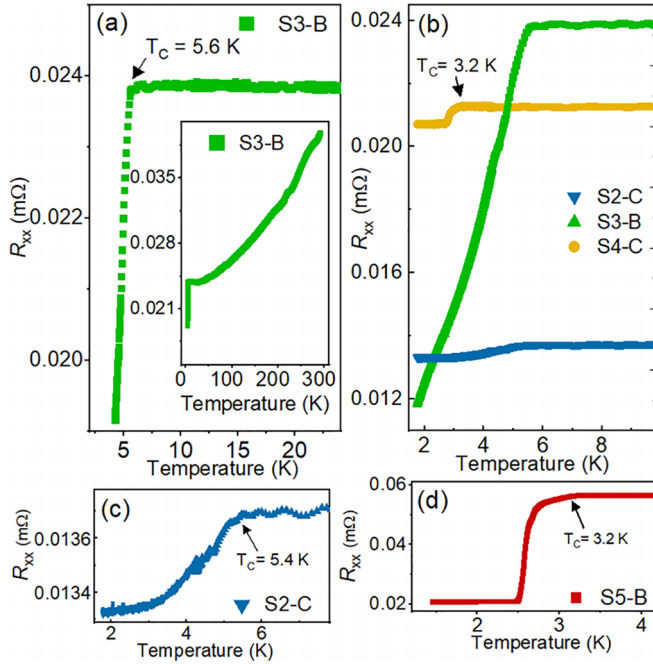


FIG. 1. Resistivity as a function of temperature of (a) S3-B with high T_c of 5.6 K, inset is the full range from 300 K to 4.2 K. (b) The three crystals from S2-C, S3-B, and S4-C. (c) Zoom-in on the transition in S2-C. (d) Lastly, the scan for the S5-B crystal.

superconducting transition at 3.2 K in the resistivity measurement. This is consistent with the expected behavior of the nominal composition of $\text{Nb}_x\text{Bi}_2\text{Se}_3$ observed in S5-B [displayed in Fig. 1(d)]. However, the transition in S4 is much more subtle, occurring over a very small range of resistivity values, in contrast to the more pronounced transition observed in S5. It is noteworthy that neither sample reaches zero resistivity.

Differential Hall resistivity $-d\rho_{yx}/dB$ as a function of the magnetic field B is displayed in Fig. 2 for three of the crystals [S2-C in (a), S3-B in (b), and S4-D in (c)] from the Hall resistance R_{yx} , which were measured in a temperature range between 1.4 and 70 K (raw data can be seen in the SM [30], Fig. S2). Shubnikov–de Haas (SdH) oscillations were observed for all samples with decreasing amplitude for increasing temperature. In (d), the SdH frequencies derived at 1.4 K (the lowest temperature) are compared. Again, S2 and S3 show similar characteristics, with frequencies at 153 and 161 T, respectively, both comparable to the value of 166 T at 1.4 K for pristine Bi_2Se_3 (value from [33]). However, S4 acts more like the doped system with a frequency of 210 T (190 T for $\text{Nb}_{0.25}\text{Bi}_2\text{Se}_3$ in [13]). The S5-B crystal also displayed SdH oscillations at 1.4 K but to a lesser degree than the substituted samples, as seen in the SM [30] (Fig. S3).

The angular dependence was investigated at 1.4 K. The results for S2-C are displayed in Fig. 2(e). (For the remaining samples, the results can be found in the SM [30].) The θ angle describes the angle between the surface normal [called “c,” since this is also the unit cell c axis of the layered structure] and the direction of the magnetic field (B) tilted from zero to 90° as a function of magnetic field up to 30 T [see illustration in Fig. 2(e)]. The SdH frequency is determined and plotted

TABLE II. T_c ’s from the susceptibility measurements on powders and transport measurements on crystals from the same areas. The last column is the content from the quantified phase analysis, with Bi_2Se_3 and misfit, and for S5-B, also BiSe . See the Experimental Methods section for information on how the T_c values were determined.

Sample	T_c (powder)	T_c (crystal)	Misfit content
S1-B	~ 3 K	1.8 K	5%
S2-C	4.5 K	5.4 K	8%
S3-B	~ 3 K	5.6 K	3%
S4-C	2.7 K	3.2 K	16%
S5-B	2.8 K	3.2 K	7% (29% BiSe)

for each angle in Fig. 3(a). A decrease in the frequency is observed with increasing angles for all three crystals. The signal-to-noise ratio is at the same time also increasing as the amplitude of the SdH oscillations decreases with increasing θ , making it challenging to define frequencies above 60° .

The Dingle temperature (T_D) for the SdH frequency was determined for each crystal in Fig. 3(b), deduced from the periodicity in the I/B dependence of the oscillation amplitude. This was calculated from the best linear fits with the function $-\pi m^*/(eT_D B)$ [see Fig. 3(b)]. A fast Fourier transform (FFT) of the amplitude is displayed in Fig. 3(c). The curves in (b) are the best fit to the data, made for the assumption that $\chi(T)/\sinh[\chi(T)]$, with $\chi(T) = (4\pi 3m^*k_B T)/(heB)$. The effective mass of the charge carriers are then determined to be $m^* \simeq 0.14 m_e$, $0.13 m_e$, and $0.15 m_e$ for the three crystals of S2-C, S3-B, and S4-C, respectively. This is again close to undoped Bi_2Se_3 of $0.16 m_e$ [33].

An estimate of the Fermi energy (E_F) (assuming a spherical Fermi surface) was conducted using the Hall data and SdH frequencies for four samples (S2 and S3 batches). For the two samples (S2-C and S3-D) without data for the temperature dependence, $m^* = 0.135 m_e$ was assumed, and the results are displayed in Fig. 4. All the E_F estimates from the Shubnikov–de Haas data are quite similar for all four samples but are more scattered for the Hall data (see Fig. S4 in the SM [30]). The reason behind this difference is unknown, but the larger value for S3-C could be due to a wrongful estimate of m^* .

B. Powder samples

The susceptibility was measured on powder extracted from various areas of the crystal boules with the results displayed in Fig. 5 (a complete investigation of each crystal boule can be found in the SM [30] in Fig. S5). The superconducting response in the susceptibility is minor for S1-B, S2-C, and S3-B (the most substituted samples, see inset for zoom-in), compared to about 100 times stronger signal for S4-C ($\text{Nb}_{0.10}\text{Bi}_{1.90}\text{Se}_3$) and S5-B ($\text{Nb}_{0.25}\text{Bi}_2\text{Se}_3$), both with clear transitions with a T_c of 2.7 K and 2.8 K, respectively. However, the susceptibility measurements were only measured down to 1.8 K, meaning the transition could appear at lower temperatures, as observed for S1-B. Hints: The samples show various superconducting behaviors. An overview of the different T_c ’s is displayed in Table II. S2-C has a broad transition starting around 4.5 K, and S1-B and S3-B have indications of transi-

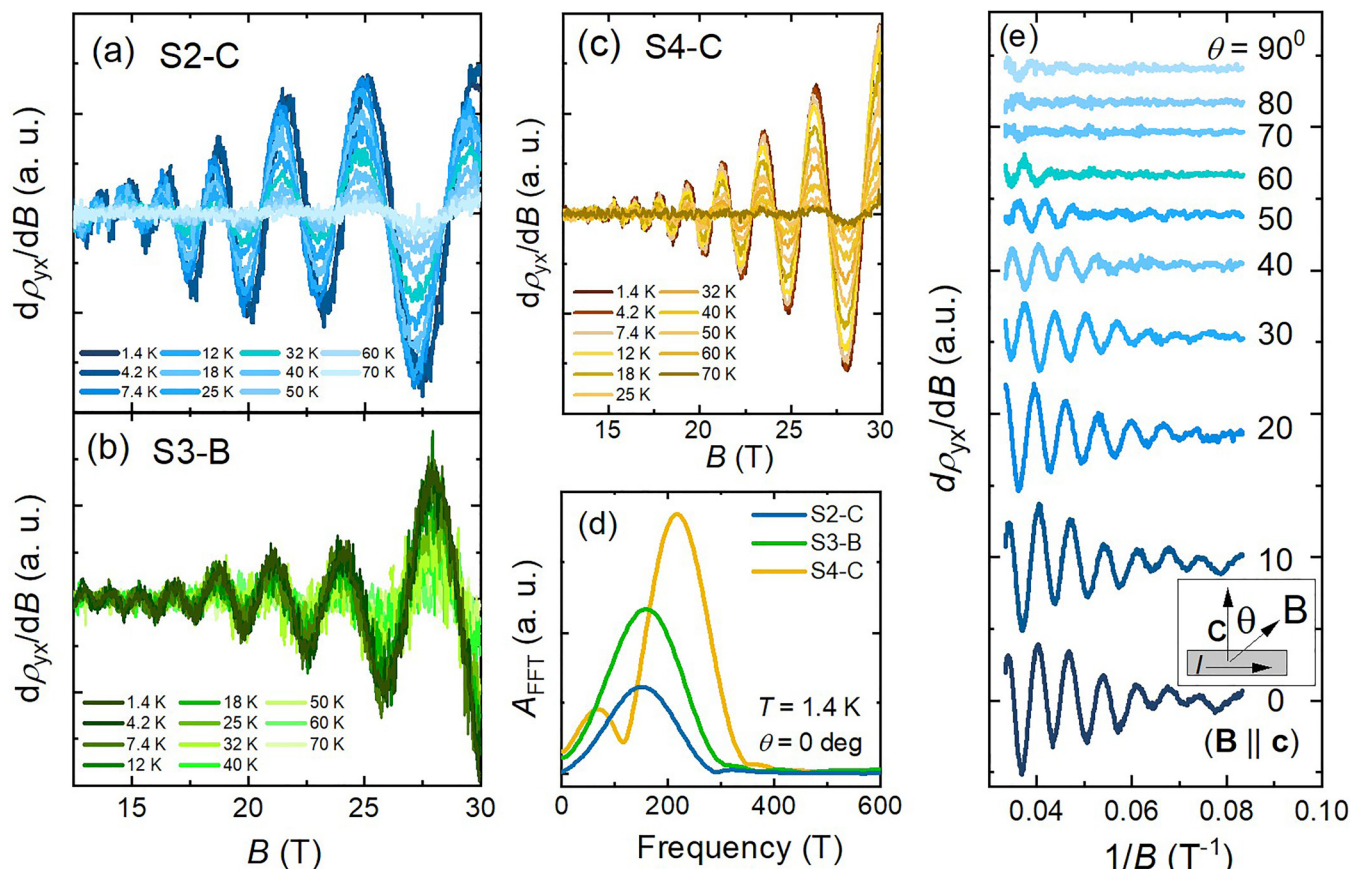


FIG. 2. Differential Hall resistivity $-d\rho_{yx}/dB$ vs magnetic field B (T) for the three crystals, (a) S2-C, (b) S3-B, and (c) S4-D. (d) The FFT amplitude of the SdH oscillations at 1.4 K (B-field interval between 12 T and 30 T), with frequencies of crystals oscillations detected to be 153 T, 161 T, and 210 T, respectively. (e) Angular dependence of the differential longitudinal resistivity of S2-C at 1.4 K, with θ from zero to 90° .

tions starting around 3 K. However, the recorded data includes a high signal-to-noise ratio, and with these weak signals, too

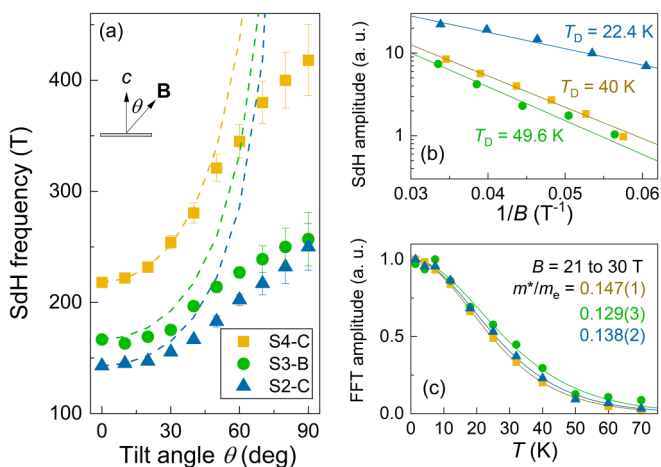


FIG. 3. (a) Angular dependence of SdH frequencies at 1.4 K for S2-C, S3-B, and S4-C. [The same color scheme is used for all plots, but only shown in (a).] (b) The extraction of the Dingle temperature (T_D) from the SdH amplitudes, $1/B$. (c) The effective mass (m^*) for three samples was calculated from the normalized FFT (fast Fourier transform) amplitude as a function of temperature (in the range $B = 21$ – 30 T).

much importance should not be given to the exact values. The powdered sample of S2-C is the only one with a T_c that resembles the transport results, but none of the recorded T_c values are close to the 5.4–5.6 K range.

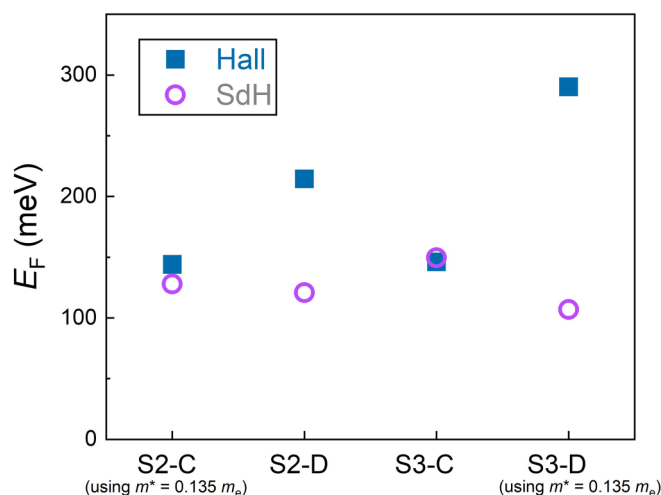


FIG. 4. An estimate of the Fermi energy (assuming a spherical Fermi surface) using the Hall data and SdH frequencies for four samples.

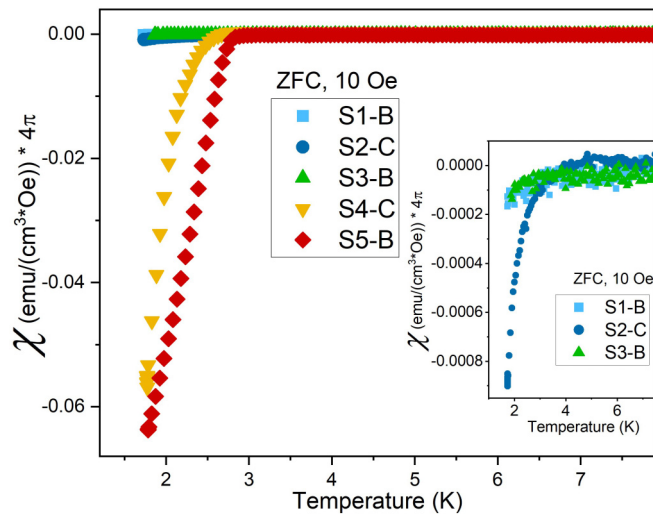


FIG. 5. Susceptibility measurements as ZFC with a magnetic field of 10 Oe on selected areas for the five samples (S1–S5). The inset shows zoom-in on the S1–S3 superconducting transitions.

A study on monolayer NbSe₂ reports how the T_c can be tuned from 4.56 K for ten-layer, 4.2 K for five-layer, to 1.0 K for monolayer NbSe₂ [34]. The misfit layer compound is reported to have significant variations in its stoichiometry, with δ in (BiSe)_{1+ δ} NbSe₂, and these variations affect the superconducting transition temperature [35]. They reported how T_c of 2.4 K was measured for $\delta = 0$, while a T_c of 3.2 K was observed for $\delta = 0.33$. This range of T_c overlaps with the typical variation observed in Nb_xBi₂Se₃ samples. This raises questions about the possible presence of nonperiodically distributed few layers of NbSe₂ or the misfit layer compound between Bi₂Se₃ layers (thus not observed in PXRD). It is also possible that the variation in δ is responsible for the

unusually high T_c values observed in S2 and S3. These effects could contribute to the broadening of the transitions and the increased T_c values.

The phase content was quantified using the same method presented and described in detail in the SM in Ref. [14], and all diffraction peaks have been described by the three phases: Bi₂Se₃, (BiSe)_{1.1}NbSe₂, and BiSe. PXRD was performed on powders from each area along each crystal boule [see Fig. 6(a)], as displayed for S2 and S5 in Fig. 6(b). Figure 6(c) shows a zoom-in on the relevant diffraction peaks. The result reveals how two phases, Bi₂Se₃ and (BiSe)_{1.1}NbSe₂ (misfit), are present along the crystal boule in S2 [see Fig. 6(d)], with surprisingly no sign of BiSe. This is different from what was discovered previously in [14] for the Nb-doped Bi₂Se₃ samples (and as for S5, as displayed), with contents up to 48% of BiSe, for areas closest to the top of the crystal boule (A-B areas). The S3 and S4 sample areas were analyzed correspondingly (see Fig. 7), where the misfit compound gradient through the crystal boules is more homogeneous than in S1 (see SM [30], Fig. S6). This sample was made before the others with a less elaborate synthesis method, as explained in the SM, which is believed to cause this difference. The pre-heating and longer heating periods were discovered to impact the crystal homogeneity hugely.

The samples with a nominal composition of Nb_{0.25}Bi_{1.75}Se₃ (S2) and the Nb_{0.20}Bi_{1.80}Se₃ (S3) obtained a steady increase in misfit phase content along the crystal boule, from 1% (area A) to 13%–18% (area D) (see Fig. 7). For S4 and S5 (Nb_{0.10}Bi_{1.90}Se₃ and Nb_{0.25}Bi₂Se₃, respectively), the phase distributions are more inhomogeneous, with all three phases being present, like what was observed previously [14]. Surprisingly, the substituted samples result in much less Nb content, accounted for in the form of a misfit phase, compared to the nominal compositions, see Table III. This suggests that the Nb could be integrating into the main structure of

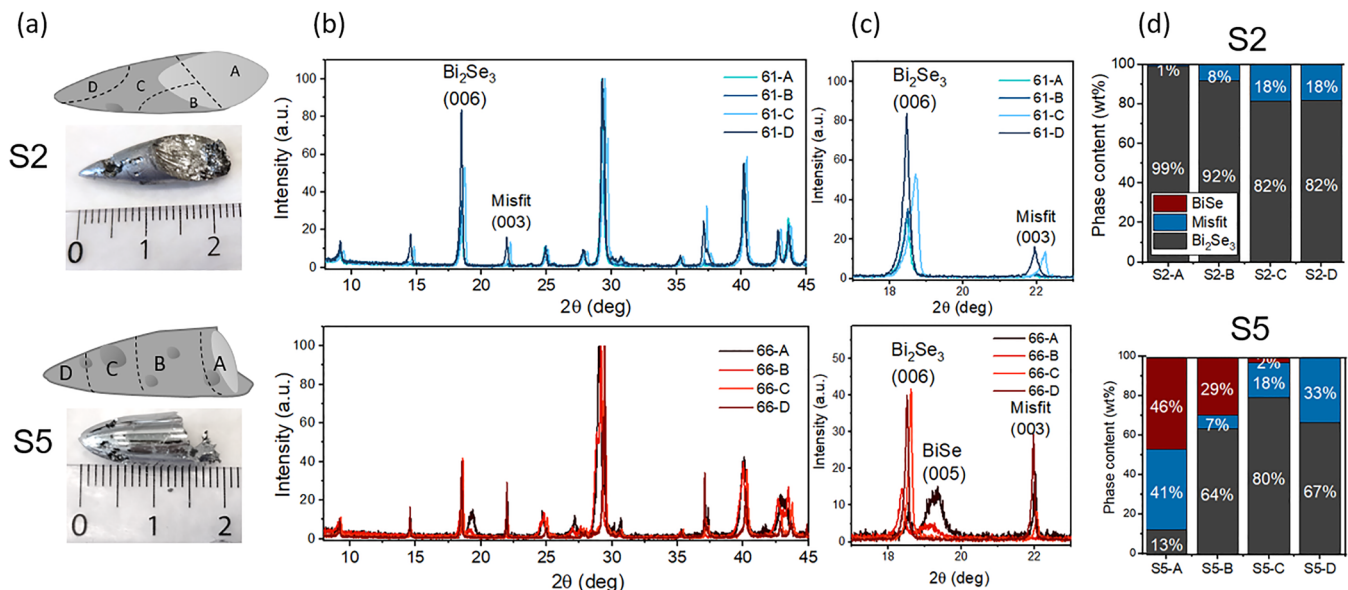


FIG. 6. (a) Pictures and illustrations of the crystal ingots of S2 and S5. (b) The powder x-ray diffraction pattern of the areas in S2 and S5. (c) Selected reflection peak positions for the three different phases known for this system, as indicated by their (hkl) indices. (d) The final results from the phase content analysis, with the amount of the different phases present in the sample areas, with Bi₂Se₃ (gray), BiSe (red), and “misfit” indicating the misfit layer compound (BiSe)_{1.1}NbSe₂ (blue).

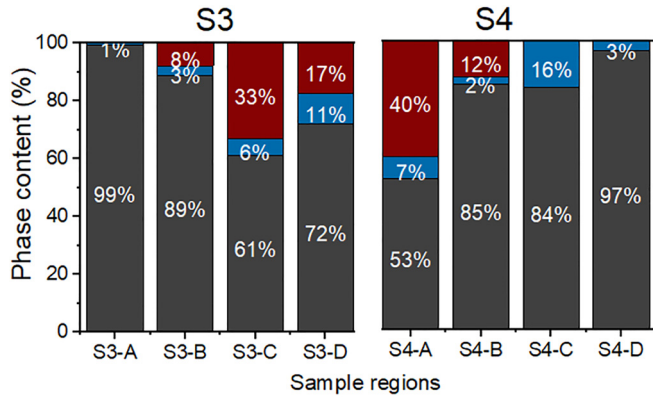


FIG. 7. Final results from the phase content analysis, with the amount of the different phases present in the different sample areas, with Bi_2Se_3 (gray), “misfit” indicating the misfit compound $(\text{BiSe})_{1,1}\text{NbSe}_2$ (blue) and BiSe (red).

Bi_2Se_3 , with less than half of Nb accounted for in S2 and S3 (as determined from the phase content analysis), or as a few layers of nonperiodically distributed between layers of Bi_2Se_3 , undetectable by PXRD.

The phase analysis does not provide a direct indication of the misfit content (in wt.%) that could explain the observed high T_c values in S2-C and S3-B (see Table II for misfit content compared with T_c 's). Speculation arises from the absence of the BiSe phase, suggesting that the efforts to substitute Bi with Nb in the Bi_2Se_3 phase were successful. However, the previous XAFS study on S1 did not display this [28]. A new study of the local structure is needed to confirm or refute this. Of high interest is the case with the strong likeness between S4 and S5 ($\text{Nb}_{0,10}\text{Bi}_{1,90}\text{Se}_3$ and $\text{Nb}_{0,25}\text{Bi}_2\text{Se}_3$, respectively), suggesting that the driving force behind the higher T_c of S2 and S3 ($\text{Nb}_{0,25}\text{Bi}_{1,75}\text{Se}_3$ and $\text{Nb}_{0,20}\text{Bi}_{1,80}\text{Se}_3$) lies more in the decrease in Bi content than in the increase of the misfit compound phase.

C. Crystal boules

The crystal homogeneity of samples S2–S5 was investigated with a potential Seebeck microprobe. After polishing the surface, the four crystal boules were scanned along the side (from top to tip). All four crystal surfaces show traces of multiple phases (see Fig. 8). The different phases are indicated by the difference in the Seebeck constant ($\mu\text{V}/\text{K}$) that appears

TABLE III. Calculated Nb contents from the nominal composition and the results from the phase analysis. This is calculated from the total amount of misfit compound phase present in the whole crystal boule, then divided into the Nb [for the assumption that Nb is a 1/5 part of misfit with composition $(\text{BiSe})(\text{NbSe}_2)$].

Crystal boule	Calc. Nb (wt.%)	Observed Nb (wt.%)
S1	4.76%	3.3(1)%
S2	5%	2.2(1)%
S3	4%	1.3(1)%
S4	2%	1.4(1)%
S5	4.76%	4.9(1)%

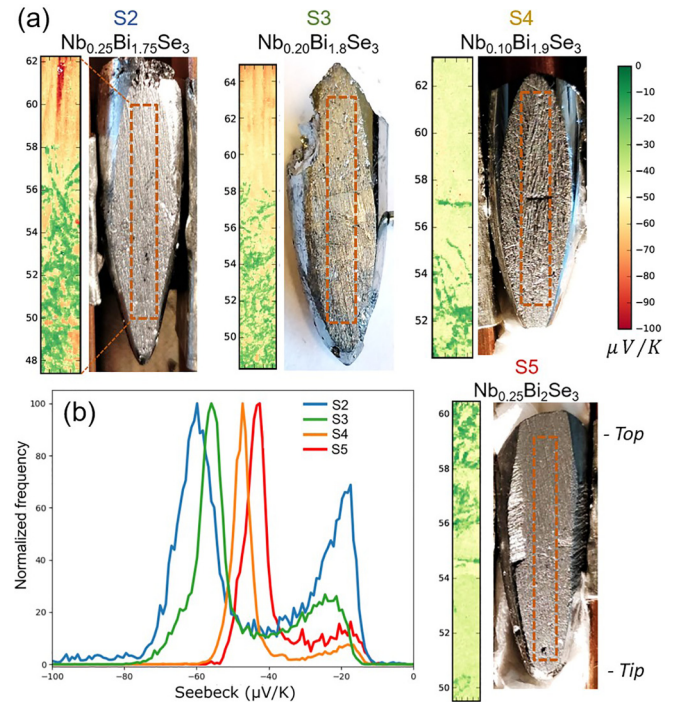


FIG. 8. (a) Seebeck measurements on samples S2–S5 with potential Seebeck microprobe (PSM), with the crystals shown next to the resulting scan, the area indicated on each. On S5, there are indications of the “top” and “tip” regions of the crystal boule. (b) The histogram for each sample for comparison.

as a color contrast. For samples S2–S4, a more negative Seebeck constant is centered at the top end (more yellow or red color) than at the tip. However, the opposite trend is spotted in S5. The reason for this difference is unknown, since all were synthesized identically, other than being an effect of the nominal composition resulting in different contents of the misfit. The overall histograms from each scan are normalized for comparison in Fig. 8(b). There is no clear gradient along the crystal boules, since the two main phases (the two maxima in the histogram) are always easily distinguishable. Still, there is a small tendency for more islands gathered of the secondary (green) phase towards the tip than the main phase, as mentioned. The tip is most likely where crystallization is initiated, as it is cooled first. This suggests that the two phases are crystallized simultaneously, intergrown or neighboring, until a point along the crystal boule (around the middle for S2 and S3, a third part up for S4), where the main phase is the vast majority above. This could be due to all the excess Nb being “used up” at this point. Looking at the results from the phase analysis would explain the tendency for the presence of the misfit compound phase (see Fig. 7) in S2 and S3. These results are only surface scans of the polished surface and do not represent the whole bulk, though the tendency is expected to be similar throughout the bulk.

IV. DISCUSSION AND CONCLUSION

Superconductivity and SdH oscillations were detected for all samples with Nb substituted for Bi. This was especially pronounced for samples with more Nb content [S2 (25%)

and S3 (20%)] that also have abnormally high T_c 's of 5.4 K and 5.6 K, not reported before for this system. The magnetotransport revealed SdH oscillations closely related to those reported for pristine Bi_2Se_3 [33]. The substituted samples with higher contents of Nb (higher x) in $\text{Nb}_x\text{Bi}_{2-x}\text{Se}_3$ (S2 and S3) were shown to have overall characteristics more like those of pristine Bi_2Se_3 , but with superconducting properties and unusually high T_c values up to 5.6 K. This is largely different from the reports on Nb-doped Bi_2Se_3 (S5, or as reported in [14]), where the properties are overall different from pristine Bi_2Se_3 , and T_c values more normalized around 3 K. The thorough study of the angular dependence of the SdH frequencies was presented together with determined Dingle temperatures and calculated m^* to estimate the Fermi energy of the system. Samples with high content of Nb show properties that generally only would appear for homogeneous and defect-free single crystals of pristine Bi_2Se_3 , however, with the superconducting response as well. For the bulk powdered samples, a broader transition into the superconducting state is observed for the substituted samples with more Nb (S2 and S3) and narrower for the sample with less Nb content (S4) and the Nb-doped Bi_2Se_3 (S5) sample. The broadening in the superconducting transition could be due to a few layers of NbSe_2 or the misfit compound in between the Bi_2Se_3 , as seen for the monolayer NbSe_2 study [34]. The high T_c 's reported here could be from unusually high δ values in $(\text{BiSe})_{1+\delta}\text{NbSe}_2$. This trend was reported in [35], and samples, corresponding to δ values in $(\text{BiSe})_{1+\delta}\text{NbSe}_2$ of 0 and 0.33, had superconducting transitions with T_c determined to be 2.3 K and 3.2 K, respectively. The actual contents (wt.%, as proposed in Refs. [14,27]) are, therefore, possibly not a sufficient explanation, but instead, it is possibly a correlation between the δ values of the misfit phase and the T_c . Further studies are necessary to more than speculate whether the T_c 's of 5.4 and 5.6 K in the substituted series could be explained by this.

Others report a tendency with an increasing amount of misfit compound phase, giving a larger superconducting response (with a larger drop in susceptibility) [27]. The misfit compound phase contents for the sample in our study are "only" 8% and 3% for S2-C ($\text{Nb}_{0.25}\text{Bi}_{1.75}\text{Se}_3$) and S3-B ($\text{Nb}_{0.20}\text{Bi}_{1.8}\text{Se}_3$), respectively, compared to samples S4-C and S5-B, with 16% and 7%. Again, we highlight how S4 ($\text{Nb}_{0.10}\text{Bi}_{1.9}\text{Se}_3$) and S5 ($\text{Nb}_{0.25}\text{Bi}_2\text{Se}_3$) display similar

properties, both in transport and susceptibility. This suggests that the driving force behind the high T_c 's lies elsewhere than in the actual amount (wt.%) of Nb (or misfit compound) in the attempted substituted samples. However, it is still evident that the main superconducting properties all arise due to the unavoidable presence of the misfit layer compound in all superconducting samples, as was also concluded from our previous studies [14,29].

This study reveals intriguing insights into the distribution of Nb in the $\text{Nb}_x\text{Bi}_{2-x}\text{Se}_3$ system. While uncertainties remain regarding the precise location of Nb atoms, the phase determination of the misfit layer compound does not account for all Nb atoms nominally added. The crystal boules were scanned by potential Seebeck measurements, revealing a tendency for a gradient of phases located at different ends of the boule, with more islands of different phases at the tip for the substituted samples. Interestingly, there are variations in the distribution of the misfit phase from the PXRD analysis, with varying amounts observed even within the same area when considering both powder and smaller single crystals. Importantly, our previous XAFS study [28] provides valuable insights into the $\text{Nb}_x\text{Bi}_2\text{Se}_3$ case, confirming that all Nb atoms are part of a NbSe_2 local environment similar to that observed in the misfit compound phase. These findings pave the way for further investigations and highlight the complex nature of the $\text{Nb}_x\text{Bi}_2\text{Se}_3$ system. For future studies, it would be interesting to spatially map the crystalline phases and the atomic Nb concentrations on scales ranging from the atomic to tens of micrometers. Such mapping could shed light on the domain sizes, how the phases stack, the distribution of Nb, and in turn the structural origin of the larger T_c 's.

ACKNOWLEDGMENTS

We gratefully acknowledge funding from VILLUM FONDEN through the Centre of Excellence for Dirac Materials (Grant No. 11744), the Danish Council for Independent Research, Natural Sciences, under the Sapere Aude program (Grant No. 7027-00077B). Affiliation with the Center for Integrated Materials Research (iMAT) at Aarhus University is gratefully acknowledged. This work was supported by HFML-RU/NWO-I, a member of the European Magnetic Field Laboratory (EMFL).

-
- [1] M. Z. Hasan and C. L. Kane, *Rev. Mod. Phys.* **82**, 3045 (2010).
- [2] Y. Ando, *J. Phys. Soc. Jpn.* **82**, 102001 (2013).
- [3] J. E. Moore, *Nature (London)* **464**, 194 (2010).
- [4] T. O. Wehling, A. M. Black-Schaffer, and A. V. Balatsky, *Adv. Phys.* **63**, 1 (2014).
- [5] Y. S. Hor, P. Roushan, H. Beidenkopf, J. Seo, D. Qu, J. G. Checkelsky, L. A. Wray, D. Hsieh, Y. Xia, S.-Y. Xu *et al.*, *Phys. Rev. B* **81**, 195203 (2010).
- [6] Y. S. Hor, A. J. Williams, J. G. Checkelsky, P. Roushan, J. Seo, Q. Xu, H. W. Zandbergen, A. Yazdani, N. P. Ong, and R. J. Cava, *Phys. Rev. Lett.* **104**, 057001 (2010).
- [7] M. Kriener, K. Segawa, Z. Ren, S. Sasaki, S. Wada, S. Kuwabata, and Y. Ando, *Phys. Rev. B* **84**, 054513 (2011).
- [8] J. A. Schneeloch, R. D. Zhong, Z. J. Xu, G. D. Gu, and J. M. Tranquada, *Phys. Rev. B* **91**, 144506 (2015).
- [9] Z. Liu, X. Yao, J. Shao, M. Zuo, L. Pi, S. Tan, C. Zhang, and Y. Zhang, *J. Am. Chem. Soc.* **137**, 10512 (2015).
- [10] Y. Pan, A. M. Nikitin, G. K. Araizi, Y. K. Huang, Y. Matsushita, T. Naka, and A. de Visser, *Sci. Rep.* **6**, 28632 (2016).
- [11] H. Leng, D. Cherian, Y. K. Huang, J.-C. Orain, A. Amato, and A. de Visser, *Phys. Rev. B* **97**, 054503 (2018).
- [12] Y. Qiu, K. Nocona Sanders, J. Dai, J. E. Medvedeva, W. Wu, P. Ghaemi, T. Vojta, and Y. San Hor, [arXiv:1512.03519](https://arxiv.org/abs/1512.03519).

- [13] B. J. Lawson, P. Corbae, G. Li, F. Yu, T. Asaba, C. Tinsman, Y. Qiu, J. E. Medvedeva, Y. S. Hor, and L. Li, *Phys. Rev. B* **94**, 041114(R) (2016).
- [14] S. M. Kevy, H. E. Lund, L. Wollesen, K. J. Dalgaard, Y.-T. Hsu, S. Wiedmann, M. Bianchi, A. J. U. Holt, D. Curcio, D. Biswas, A. J. H. Jones, K. Volckaert, C. Cacho, P. Dudin, P. Hofmann, and M. Bremholm, *Phys. Rev. B* **103**, 085107 (2021).
- [15] M. P. Smylie, H. Claus, U. Welp, W.-K. Kwok, Y. Qiu, Y. S. Hor, and A. Snezhko, *Phys. Rev. B* **94**, 180510(R) (2016).
- [16] T. Asaba, B. J. Lawson, C. Tinsman, L. Chen, P. Corbae, G. Li, Y. Qiu, Y. S. Hor, L. Fu, and L. Li, *Phys. Rev. X* **7**, 011009 (2017).
- [17] S. Sasaki, M. Kriener, K. Segawa, K. Yada, Y. Tanaka, M. Sato, and Y. Ando, *Phys. Rev. Lett.* **107**, 217001 (2011).
- [18] S. Sasaki and T. Mizushima, *Physica C* **514**, 206 (2015).
- [19] A. Kitaev, *Ann. Phys.* **303**, 2 (2003).
- [20] P. Zhang, K. Yaji, T. Hashimoto, Y. Ota, T. Kondo, K. Okazaki, Z. Wang, J. Wen, G. D. Gu, H. Ding *et al.*, *Science* **360**, 182 (2018).
- [21] J. Zhang, J. Sun, Y. Li, F. Shi, and Y. Cui, *Nano Lett.* **17**, 1741 (2017).
- [22] Z. Li, M. Wang, D. Zhang, N. Feng, W. Jiang, C. Han, W. Chen, M. Ye, C. Gao, J. Jia *et al.*, *Phys. Rev. Mater.* **2**, 014201 (2018).
- [23] K. Kobayashi, T. Ueno, H. Fujiwara, T. Yokoya, and J. Akimitsu, *Phys. Rev. B* **95**, 180503(R) (2017).
- [24] Y. Gotoh, M. Onoda, K. Uchida, Y. Tanaka, T. Iida, H. Hayakawa, and Y. Oosawa, *Chem. Lett.* **18**, 1559 (1989).
- [25] W. Y. Zhou, A. Meetsma, J. L. de Boer, and G. A. Wiegers, *Mater. Res. Bull.* **27**, 563 (1992).
- [26] A. Nader, A. Briggs, and Y. Gotoh, *Solid State Commun.* **101**, 149 (1997).
- [27] M. E. Kamminga, M. Batuk, J. Hadermann, and S. J. Clarke, *Commun. Mater.* **1**, 82 (2020).
- [28] K. J. Dalgaard, S. M. Kevy, L. Wollesen, Q. Ma, S. Wiedmann, K. G. V. Sigfridsson Clauss, and M. Bremholm, *Phys. Rev. B* **103**, 184103 (2021).
- [29] S. M. Kevy, L. Wollesen, and M. Bremholm, *J. Solid State Chem.* **330**, 124477 (2024).
- [30] See Supplemental Material at <http://link.aps.org/supplemental/10.1103/PhysRevMaterials.8.054801> for further information about synthesis procedures and details about physical properties obtained from transport and susceptibility measurements.
- [31] P. Ziolkowski, G. Karpinski, T. Dasgupta, and E. Müller, *Phys. Status Solidi A* **210**, 89 (2013).
- [32] G. R. Hyde, H. A. Beale, I. L. Spain, and J. A. Woollam, *J. Phys. Chem. Solids* **35**, 1719 (1974).
- [33] M. Busch, O. Chiatti, S. Pezzini, S. Wiedmann, J. Sánchez-Barriga, O. Rader, L. V. Yashina, and S. F. Fischer, *Sci. Rep.* **8**, 485 (2018).
- [34] H. Wang, X. Huang, J. Lin, J. Cui, Y. Chen, C. Zhu, F. Liu, Q. Zeng, J. Zhou, P. Yu *et al.*, *Nat. Commun.* **8**, 394 (2017).
- [35] M. Nagao, A. Miura, Y. Horibe, Y. Maruyama, S. Watauchi, Y. Takano, and I. Tanaka, *Solid State Commun.* **321**, 114051 (2020).